Supporting Information

MRI-activated magnetoelectric nanoparticles as theranostic agents

Martina Lenzuni[1§], Denise Galante[2§], Ilaria Faricelli[1,3], Serena Fiocchi[1], Emma Chiaramello[1], Cristina D'Arrigo[2], Roberta Tasso[4,5], Maria Chiara Ciferri[4,5], Rodolfo Quarto[4,5], Riccardo Marongiu[1], Roberta Resaz[5], Federico Zaottini[5,6], Riccardo Picasso[5], Carlo Martinoli[5,6], Paolo Ravazzani[1], Paolo Giannoni[4], Alessandra Marrella[1*].

[1] Institute of Electronics, Computer and Telecommunication Engineering, National Research Council of Italy (CNR-IEIIT), Genoa, Italy

[2] Institute of Chemical Sciences and Technologies "Giulio Natta", National Research Council of Italy (CNR-SCITEC), Genoa, Italy

[3] Department of Informatics, Bioengineering, Robotics and Systems Engineering (DIBRIS), University of Genoa, Genoa, Italy

[4] Department of Experimental Medicine (DIMES), University of Genoa, Genoa, Italy

[5] IRCCS Ospedale Policlinico San Martino, Genoa, Italy

[6] Department of Health Sciences (DISSAL), Radiology Section, University of Genoa, Genoa, Italy

§ These authors contributed equally to the work.

** correspondence: alessandra.marrella@cnr.it*

Materials and Methods

To confirm the MRI responsiveness of the MENPs, a complementary pre-clinical phantom study was carried out at 7 T using agarose gel matrices MENPs were dispersed in 1% (w/v) agarose solution at final concentrations of 0, 100, 300, 600 and 1200 μg/mL. The mixtures were poured into 1-well Nunc Lab-Tek chamber slide systems (Thermo Fisher, Waltham, USA) and allowed to solidify at room temperature. MRI acquisitions were performed using a 7T pre-clinical scanner (PharmaScan, Bruker, Germany), equipped with a 40 mm diameter transmit-receive volume coil to ensure a homogeneous signal excitation and detection. T2-weighted multi-gradient echo (MGME) sequences were acquired in the axial plane with the following parameters: repetition time (TR) = 1150 ms; number of echoes = 8; first echo time

(TE_1) = 4 ms; echo spacing = 5 ms; flip angle = 50°; field of view (FOV) = 28 mm × 28 mm; matrix size = [256 x 256; slice thickness = 0.8 mm; number of averages = 2.

Quantitative relaxometry was used to determine T2* relaxation times, and the corresponding transverse relaxation rates (1/T2*) were then calculated to evaluate signal decay as a function of particle concentration. Data were analyzed using GraphPad Prism. Values were compared across six experimental groups using one-way ANOVA, which revealed a highly significant overall difference ($p < 0.0001$). A test for linear trend was applied to verify whether transverse relaxation rate values increased progressively with concentration. The trend was statistically significant ($p < 0.0001$), with a positive slope indicating a clear increase in 1/T2* as particle concentration rose. This pattern supports the expected effect of MENPs in shortening transverse relaxation.

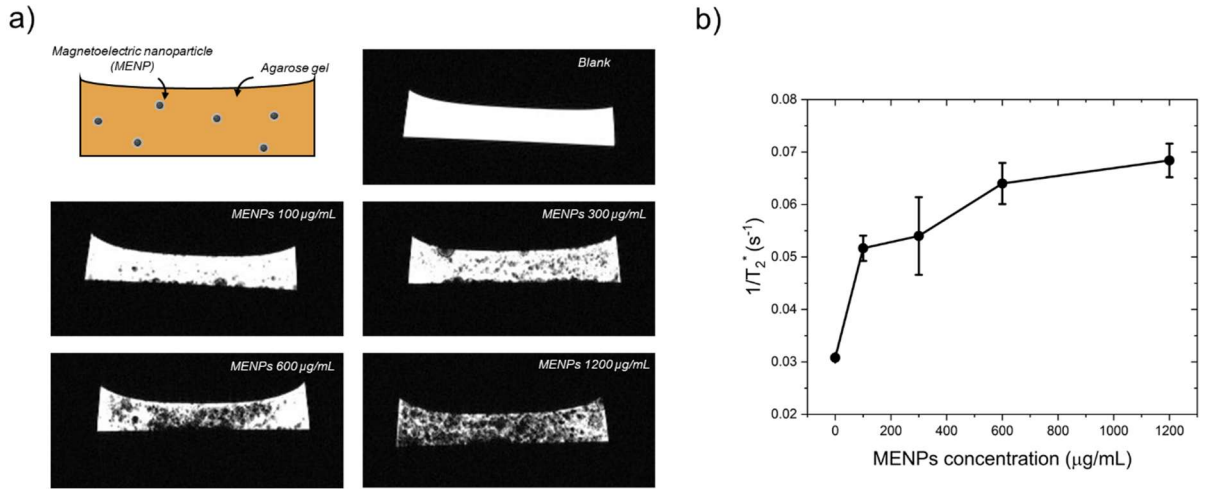

Figure S1. MRI responsiveness of MENPs with a 7T system. a) MRI phantom images of agarose gel-filled chamber slides containing increasing concentrations of MENPs, showing signal intensity changes corresponding to nanoparticle content. b) Quantification of relaxation rates ($1/T_2^*$) as a function of MENP concentration, confirming MRI responsiveness.

Table S1. Materials properties used in COMSOL Multiphysics environment for cobalt ferrite, barium titanate and cell culture medium.

Domain	Designation	Value	Unit	Reference
Cobalt ferrite ($CoFe_2O_4$)	Density	5200	Kg/m^3	(Fiocchi et al., 2022)
	Relative permittivity	10	-	(Carvalho et al., 2018)
	Electrical conductivity	10^{-5}	S/m	(Gopalan et al., 2009; Nlebedim and Jiles, 2014)
	Poisson ratio	0.48	-	(Fiocchi et al., 2022)
	Young's modulus	$230*10^9$	Pa	(Fiocchi et al., 2022)
	Magnetic susceptibility	0.42	-	Provided by manufacturer's measurements
	Magnetic saturation	$7.7*10^4$	A/m	Provided by manufacturer's measurements
	Saturation magnetostriction	-200	ppm	(Fiocchi et al., 2022)
Barium titanate ($BaTiO_3$)	Density	5700	Kg/m^3	COMSOL library
	Relative permittivity	{1115.1, 1115.1, 1251.3}	-	COMSOL library
	Electrical conductivity	178.5	S/m	COMSOL library
	Elasticity matrix, Voigt notation	{150.4; 65.6; 150.4; 65.; 65.9; 145.5; 0; 0; 0; 43.9; 0; 0; 0; 0; 43.9; 0; 0; 0; 0; 0; 42.4}	GPa	COMSOL library
Cell medium	Relative permeability	1	-	(Krichen et al., 2017)
	Relative permittivity	80	-	(Oh et al., 2023)
	Electrical conductivity	2	S/m	(Mazzoleni et al., 1986)

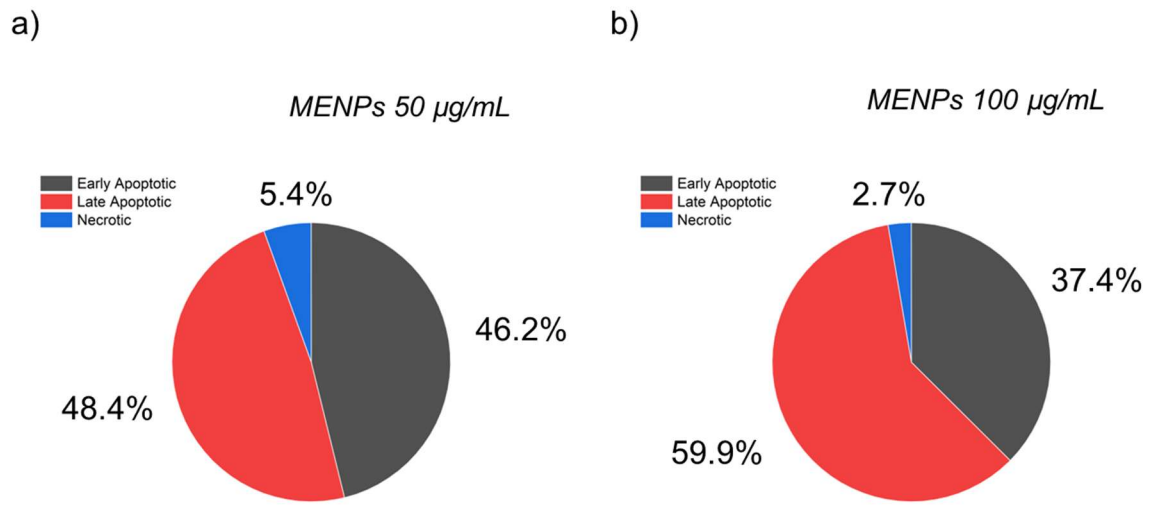

Figure S2. Assessment of cell death pathways induced by MRI-activated MENPs. Quantitative distribution of the non-viable cell population for the 50 µg/mL (a) and 100 µg/mL (b) MENP-treated groups, expressed as a percentage of total non-viable cells at T4.

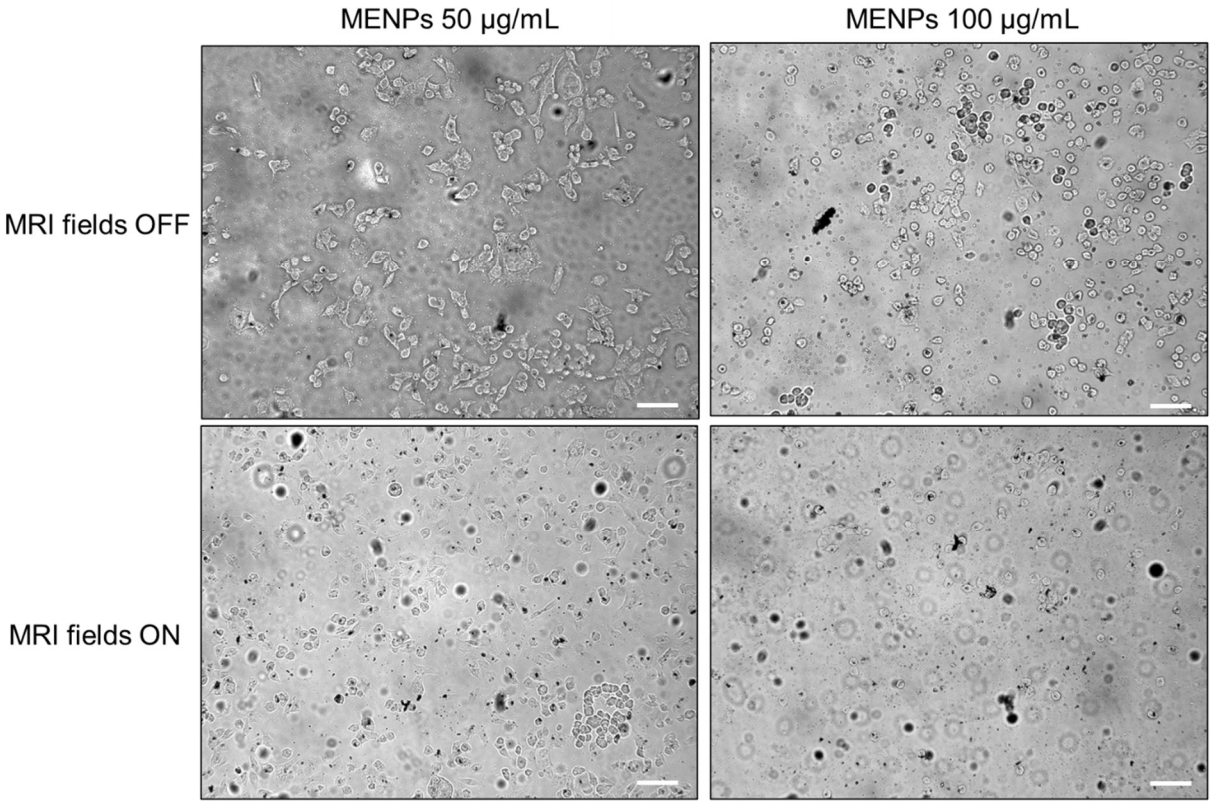

Figure S3. Brightfield images of HT-29 cells acquired at 24 hours post-exposure (T4), following treatment with MENPs at 50 µg/mL and 100 µg/mL, with MRI fields ON or OFF. Scale bar = 20 µm.

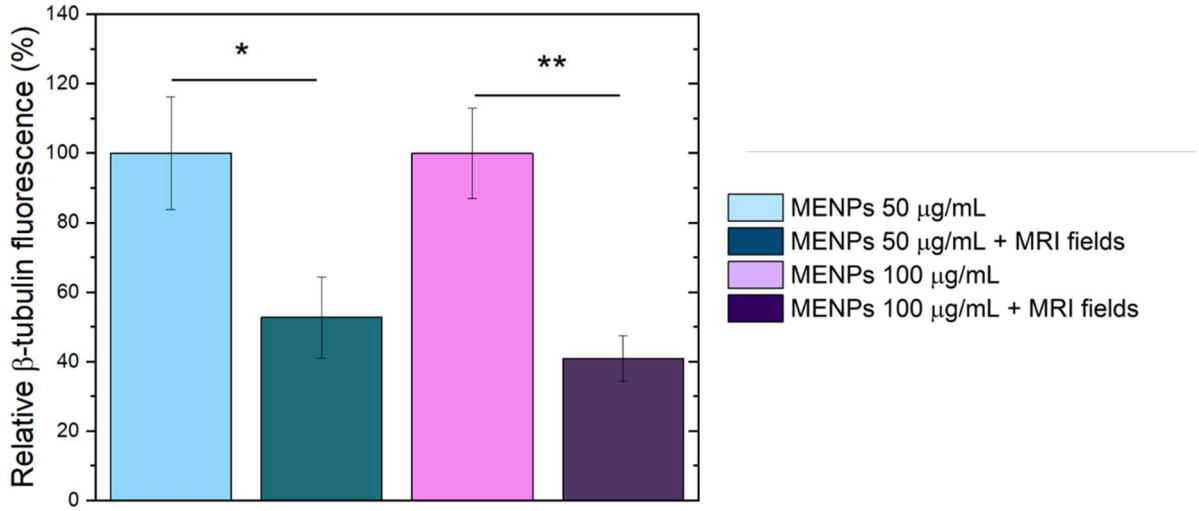

Figure S4. Quantification of β-tubulin fluorescence intensity in cells treated with MENPs (50 and 100 µg/mL) with and without MRI field exposure. Data are expressed as relative fluorescence (%) compared to cells not subjected to MRI fields. Values represent mean ± SD (n=3); * $p < 0.05$, ** $p < 0.01$.

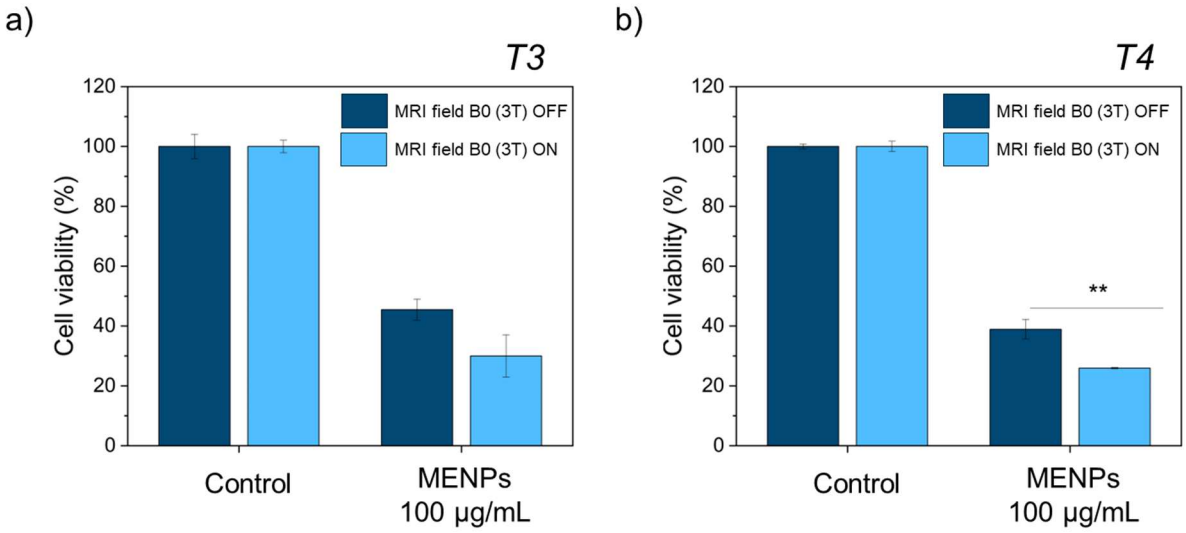

Figure S5. Effect of static magnetic field exposure on cell viability of HT-29 cells treated with MENPs. Cell viability of HT-29 cells incubated with or without MENPs (100 µg/mL), evaluated (a) immediately after exposure to a static magnetic field (3T, B_0) and (b) 24 hours later (T3 and T4, respectively). Cells were either exposed to the magnetic field (MRI field ON) or kept under identical conditions without magnetic field exposure (MRI field OFF). Data are presented as mean ± standard deviation (n = 3). Statistical significance was evaluated using Student's *t*-test. ** $p<0.01$.

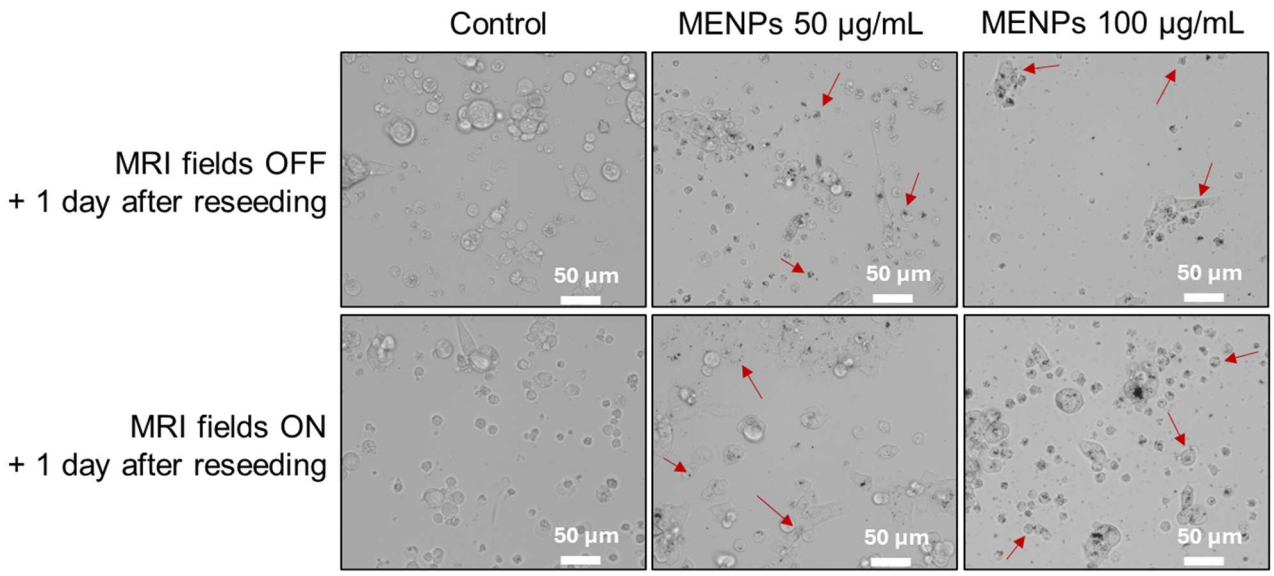

Figure S6. Optical microscopy images of HT-29 suspended cells one day after being reseeded. Each image corresponds to a specific MENPs concentration and MRI exposure condition (MRI fields ON or MRI fields OFF) and illustrates whether non-adherent cells retained viability and were able to reattach to the well surface. Red arrows indicate representative examples of MENPs internalized by the cells.

References

Carvalho, F.E., Lemos, L.V., Migliano, A.C.C., Machado, J.P.B., Pullar, R.C., 2018. Structural and complex electromagnetic properties of cobalt ferrite (CoFe2O4) with an addition of niobium pentoxide. Ceramics International 44, 915–921. https://doi.org/10.1016/j.ceramint.2017.10.023

Fiocchi, S., Chiaramello, E., Marrella, A., Suarato, G., Bonato, M., Parazzini, M., Ravazzani, P., 2022. Modeling of core-shell magneto-electric nanoparticles for biomedical applications: Effect of composition, dimension, and magnetic field features on magnetoelectric response. PLOS ONE 17, 1–17. https://doi.org/10.1371/journal.pone.0274676

Gopalan, E.V., Joy, P.A., Al-Omari, I.A., Kumar, D.S., Yoshida, Y., Anantharaman, M.R., 2009. On the structural, magnetic and electrical properties of sol–gel derived nanosized cobalt ferrite. Journal of Alloys and Compounds 485, 711–717. https://doi.org/10.1016/j.jallcom.2009.06.033

Krichen, S., Liu, L., Sharma, P., 2017. Biological cell as a soft magnetoelectric material: Elucidating the physical mechanisms underpinning the detection of magnetic fields by animals. Phys. Rev. E 96, 042404. https://doi.org/10.1103/PhysRevE.96.042404

Mazzoleni, A.P., Sisken, B.F., Kahler, R.L., 1986. Conductivity values of tissue culture medium from 20°C to 40°C. Bioelectromagnetics 7, 95–99. https://doi.org/10.1002/bem.2250070111

Nlebedim, I.C., Jiles, D.C., 2014. Suitability of cation substituted cobalt ferrite materials for magnetoelastic sensor applications. Smart Materials and Structures 24, 025006. https://doi.org/10.1088/0964-1726/24/2/025006

Oh, G., Jo, Y., Gi, Y., Hong, J., Kim, J., Lee, B., Yoon, M., 2023. Correlation between impulse magnitude and inhibition of cell proliferation in alternating electric fields therapy. AIP Advances 13, 085005. https://doi.org/10.1063/5.0153374